



ELSEVIER

15 May 1995

OPTICS  
COMMUNICATIONS

Optics Communications 117 (1995) 102–106

# A simple method to determine the effective stimulated emission cross-section of laser media

E.P. Maldonado, N.D. Vieira Junior

*Instituto de Pesquisas Energéticas e Nucleares – CNEN/SP, Supervisão de Materiais Optoeletrônicos – MMO,  
Caixa Postal 11049, CEP 05422-970, São Paulo/SP, Brazil*

Received 21 November 1994

---

## Abstract

We describe a simple method for the determination of the stimulated emission cross-section of laser media. It is based on the analysis of the laser output power as a function of the output coupling, using an acousto-optical modulator to change the equivalent output reflectivity. The effective emission cross section can be obtained from a laser oscillation model. This method allows the determination of the emission cross section by two independent parameters, the gain and the output power. The procedure was applied for an Nd:YLF laser, where the  $\pi$  ( $\lambda = 1047$  nm) and  $\sigma$  ( $\lambda = 1053$  nm) emission cross-sections were obtained, resulting in  $\sigma_{\pi} = 3.1(2) \times 10^{-19}$  cm<sup>2</sup>, and  $\sigma_{\sigma} = 1.9(2) \times 10^{-19}$  cm<sup>2</sup>, respectively.

---

## 1. Introduction

In spite of the vital importance of the effective stimulated cross-section, its precise measurement is commonly a nontrivial work, and usually appreciable differences are found among the values listed in the literature for the same material. For instance, the determined values of the 1064 nm emission cross section of Nd:YAG are in the range of  $2.7$  to  $8.8 \times 10^{-19}$  cm<sup>2</sup> [1,2]. The three main techniques used for the determination of the emission cross-section are: the reciprocity method [3,4], the Füchtbauer–Ladenburg equation [5,6], and measurements of the gain.

The gain measurement is a direct method to obtain the stimulated emission cross-section and there are several techniques to do it. The pump-and-probe technique is commonly used to determine both the small-signal gain [7] or the saturation fluence [8], thus allowing a calculation of the emission cross-section using simple

models. Both methods are reliable, with a typical precision in the range of 10–20%, and can be used in a large range of materials. However, to determine the stimulated emission cross-section of a material that already shows laser action, the simplest approach is to analyze the output power using the convenient laser model.

The small-signal gain of a laser can be experimentally determined from the delay to the onset of laser oscillation, relative to the pumping. This method avoids the complexity of the analysis of pumping conditions, even in pulsed lasers. It has been used in order to determine the effective emission cross-section by using a one-dimensional model to the laser oscillation [9]. Although this experiment can be easily analyzed, the experimental technique requires temporal resolution.

For longitudinally pumped lasers, there are reliable models for the output power [10,11]. In this case, with the knowledge of pumping and cavity parameters, it

has been shown that the emission cross-section can be determined by analyzing the absorbed pump power at threshold, with a precision of 20% [12].

In this work we demonstrate a method of emission cross-section determination using a laser model analysis, where all the laser output power range is relevant, not only the threshold of oscillation. We have used basically a one-dimensional laser oscillation model, that describes very well the output power dependence with the mirror transmission [5,13]. The double-pass cavity losses and small-signal power gain can be determined from the fitting of a theoretical expression to the experimental data. The effective emission cross-section is a third parameter obtained from this analytical fit, if the beam area inside the laser medium is approximately constant and known with some accuracy. A second cross-section determination can also be obtained, by analyzing the previous determined value of small-signal power gain, using a standard model of longitudinal gaussian pumping [10]. The precision in the cross-section determination is also increased by repeating the described procedures at different pump power levels. The experimental data were obtained by monitoring the laser output power while an intracavity acousto-optical modulator varies the output reflectivity [12]. We have used this very simple method to obtain the 1053 nm ( $\sigma$ ) and 1047 nm ( $\pi$ ) emission cross-sections of Nd:YLF.

It must be stressed that the determination of the stimulated emission cross section during the laser action leads to the *effective* value of it, regarding all transitions that contribute to the laser amplification.

## 2. Laser system configuration

The active medium samples were obtained from a Nd:YLF crystal grown in our labs, in the (1, 1, 0) direction. The Nd concentration is 0.6(1) mol% ( $0.85 \times 10^{20} \text{ cm}^{-3}$ ). Two samples were prepared (extracted along the growth direction) consisting in rectangular prisms with cross-section ( $3 \times 3$ ) mm<sup>2</sup> and length  $l = 33$  mm. The optical faces are at the Brewster angle, one for the  $\pi$  and the other for the  $\sigma$  polarization, and polished to a surface flatness of  $\lambda/10$ . The transmission of the prepared samples at  $\lambda = 1.06 \text{ }\mu\text{m}$  was 0.995(5).

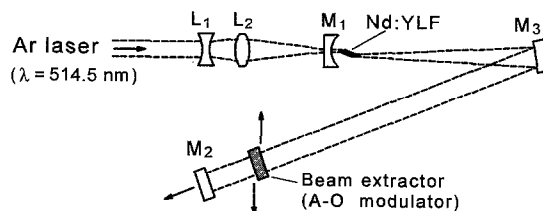


Fig. 1. General scheme of the Nd:YLF resonator. The lenses  $L_1$  and  $L_2$  are used to modermatch the pumping beam.

A three-mirror resonator was used, with astigmatic compensation, permitting a very tight beamwaist in the active medium region (Fig. 1). The mirror  $M_1$ ,  $M_2$  and  $M_3$ , have radius  $\rho_1 = 5 \text{ cm}$ ,  $\rho_2 = \infty$  and  $\rho_3 = 100 \text{ cm}$ ;  $M_1$  and  $M_3$  are highly reflecting reflectors for the emission region ( $R_{1,3} \geq 0.995$ ) and  $M_1$  has high transmission at 514.5 nm (dichroic mirror). The  $M_2$  reflectivity is 96%. The incidence angle on  $M_3$  must be  $10^\circ$  in order to compensate the astigmatism. The distance between  $M_1$  and  $M_3$  is 52.4 cm; between  $M_2$  and  $M_3$  is 97.6 cm. Thus, the beamwaist at the laser medium is  $w_0 \approx 93 \text{ }\mu\text{m}$ .

We used an argon ion laser, at  $\lambda_p = 514.5 \text{ nm}$ , as a pump source for the Nd:YLF laser. At this wavelength, the absorption coefficient is  $\alpha_a = 0.18(2) \text{ cm}^{-1}$  for the  $\sigma$  polarization and  $\alpha_a = 0.30(2) \text{ cm}^{-1}$  for the  $\pi$  polarization. The low absorption coefficient was compensated using long samples ( $l = 33 \text{ mm}$ ). The pump beam was conveniently focused to match the resonator's TEM<sub>00</sub> mode at the pumping wavelength. The geometry of the laser and pump beam at the active medium region is shown in Fig. 2.

## 3. Experimental procedure and results

A traveling-wave acousto-optic Bragg modulator [14] was inserted into the Nd:YLF cavity, near the output mirror  $M_2$  (see Fig. 1). The modulator was operated in a cw mode, extracting a fraction of the intracavity power into two additional output beams, depending on the radio-frequency amplitude. The total extracted power defines an effective reflectivity. Thus, we could change continuously the output effective reflectivity,  $R$ , while the laser output power,  $P_{\text{out}}$ , was monitored using a Ge detector connected to a lock-in amplifier. The radio-frequency amplitude and the lock-

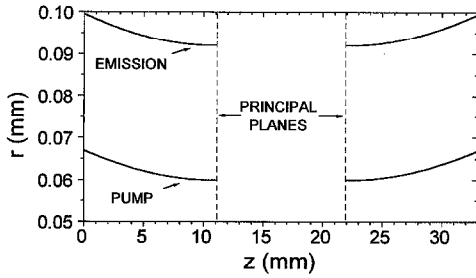


Fig. 2. Waist of the resonator's TEM<sub>00</sub> mode (EMISSION) and the pumping beam (PUMP) inside the gain medium. The pump beam profile was measured using the knife-edge method.

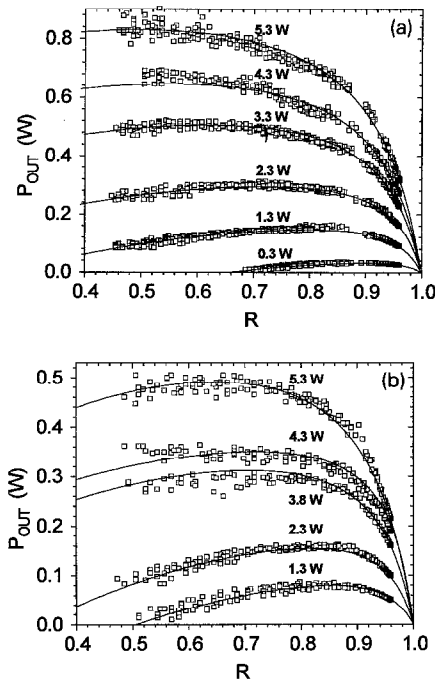


Fig. 3. Laser output power versus reflectivity, at some different pump power levels, for the  $\pi$  (a) and  $\sigma$  (b) polarization. The theoretical fitted curves are also shown.

in output were recorded in a PC micro-computer, using an analog–digital interface. The output power as a function of the output reflectivity curves were obtained for different values of pump power, for the  $\sigma$  and the  $\pi$  polarizations (the laser polarizations is coincident with the pump polarization, in both cases). Some of these sets of data are shown in Fig. 3a and 3b.

The round-trip logarithmic unsaturated gain,  $\Gamma^0$ , the round-trip logarithmic cavity losses,  $L$ , and the effective stimulated emission cross-section,  $\sigma_s$ , were

obtained performing a fit of the following theoretical expression [13]:

$$P_{\text{out}} = A \frac{h\nu}{\tau\sigma_s} \frac{-\ln(R)}{2} \left( \frac{\Gamma^0}{L - \ln(R)} - 1 \right), \quad (1)$$

where  $A$  is the average (emission) beam area within the active medium,  $h\nu = 1.9 \times 10^{-19}$  J is the photon energy,  $\tau \approx 530 \mu\text{s}$  is the Nd:YLF upper laser level lifetime for the present Nd<sup>3+</sup> concentration [15].

The obtained values for the double-pass intracavity losses are  $L = 0.05(1)$ , and they are nearly constant over all the pump power range and polarizations studied. The gain values determined are shown in Fig. 4, for both polarizations, as a function of the pump power. Fig. 5 presents the obtained values for the effective emission cross-section and the calculated averages (flat lines):  $\sigma_s = 3.0(2) \times 10^{-19} \text{ cm}^2$ , for the  $\pi$  polarization,

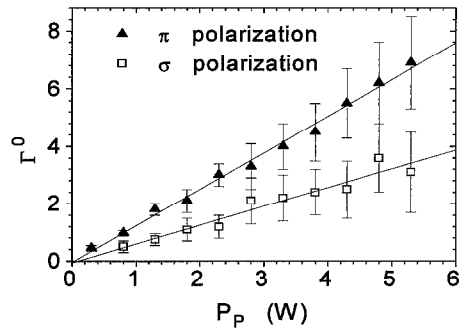


Fig. 4. Double-pass logarithmic unsaturated power gain, as a function of the pump power,  $P_p$ , for both polarizations. It is also shown the best fit of a linear expression to the data.

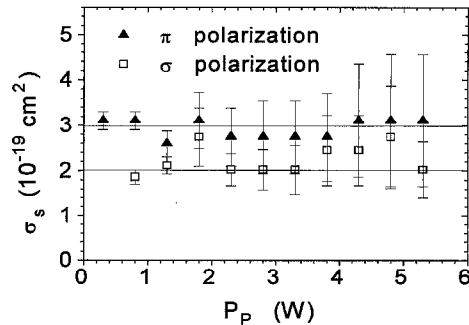


Fig. 5. Values of the Nd:YLF effective stimulated emission cross-section, for both polarizations (1047 and 1053 nm transitions), obtained from the fit of the theoretical expression 1 to the measured data (Fig. 3), for various pump power levels. It is also shown the calculated average values (straight lines).

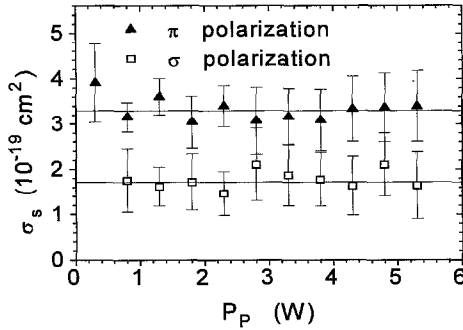


Fig. 6. Values of the Nd:YLF effective stimulated emission cross-section, for both polarizations (1047 and 1053 nm transitions), applying expression (3) to the obtained small-signal gain values, for various pump power levels. The calculated averages are the straight lines.

and  $\sigma_s = 2.0(2) \times 10^{-19} \text{ cm}^2$ , for the  $\sigma$  polarization.

A second determination of the effective emission cross-section can be carried out from the values of small-signal gain obtained, using the well-known expression from the model of longitudinal gaussian pumping [10]:

$$\Gamma^0 = P_p [1 - \exp(-\alpha_a l)] \frac{4(\lambda_p/\lambda)\beta}{\pi(w_0^2 + w_p^2)I_s}, \quad (2)$$

where  $P_p$  is the pump power,  $I_s = h\nu/\sigma_s\tau$  is the saturation intensity, and  $\beta$  is the thermal population distribution factor for the  $\sigma$  and  $\pi$  metastable state. The values of  $\beta$ , calculated at room temperature (300 K), are:  $\beta = 0.43$ , for the  $\pi$  polarization, and  $\beta = 0.57$ , for the  $\sigma$  polarization. Therefore, using expression (2) and the data for the argon laser pumped Nd:YLF laser:  $\Gamma^0 = \kappa P_p$ , where  $\kappa = \sigma_s/(2.6 \times 10^{-19})$ , for the  $\pi$  polarization, and  $\kappa = \sigma_s/(2.8 \times 10^{-19})$ , for the  $\sigma$  polarization.

Fig. 6 shows the effective emission cross-section values, calculated using the expression (3) and the data of Fig. 4. The calculated averages values (straight lines) are  $\sigma_s = 3.3(2) \times 10^{-19} \text{ cm}^2$ , for the  $\pi$  polarization, and  $\sigma_s = 1.7(2) \times 10^{-19} \text{ cm}^2$ , for the  $\sigma$  polarization.

#### 4. Discussion

The accuracy of the determined values for the  $\pi$  and  $\sigma$  stimulated emission cross sections depends obvi-

ously on how well the system is described by the simple laser model used [16].

The *low gain* approximation is valid in the present analysis because the system was studied only up to 50% of output transmission, privileging the high reflectivity data. The *Gaussian profiles of pump and emission beams* were not considered in the main analysis, but the parameters obtained agree very well with the pump expression that take it into account.

The measurement of the laser spectrum reveals, in our system, the presence of, at least, five simultaneously oscillating longitudinal modes<sup>1</sup>, as shown in Fig. 7. Considering that the simultaneous oscillation of these modes homogenizes the longitudinal distribution of gain saturation, the effect of *longitudinal spatial hole burning* is not a source of error in this case [16]. The *hole-burning* modes frequency separation is given by the relation [17]:  $\Delta\nu_{\text{hb}} \cong c/(4d)$ , where  $c$  is the velocity of light and  $d$  is the distance of the active medium to the resonator end. In our case, this is the distance to mirror  $M_1$ :  $d \cong 2 \text{ cm}$ . Thus, the frequency separation is  $\Delta\nu_{\text{hb}} \cong 3.8 \text{ THz}$ , or  $0.13 \text{ cm}^{-1}$ .

For the present laser system, the observed output power can be completely described using the model (see Fig. 3), for the range of reflectivities studied. The system parameters, obtained from the fit of the theoretical expression, match very well the values obtained from direct measurements (system losses, pumping power and geometry, etc.).

<sup>1</sup> We have used a 1 m SPEX spectrometer. The hole-burning modes spectral shape could not be resolved due to effects of spectral thermal drift (of the laser).

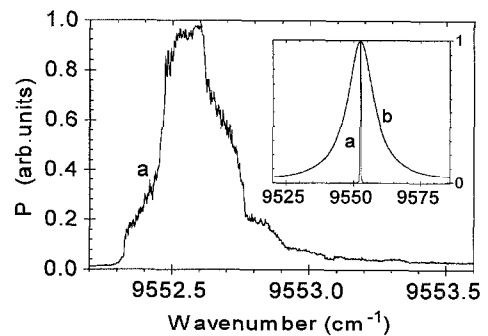


Fig. 7. Time averaged laser output power spectrum (curves labeled a) measured for the Nd:YLF laser system used, indicating the presence of (at least) five hole-burning modes. It is also shown (insert) the fluorescence lineshape (curve b).

Finally, we prefer to assume the determined values of the Nd:YLF cross-sections as the average of the values obtained from the two independent parameters. Thus,  $\sigma_s = 3.1(2) \times 10^{-19} \text{ cm}^2$ , for the  $\pi$  polarization, and  $\sigma_s = 1.9(2) \times 10^{-19} \text{ cm}^2$ , for the  $\sigma$  polarization. Usually, the reported values for these cross-sections of Nd:YLF are in the range of  $1.9 \times 10^{-19} \text{ cm}^2$  up to  $3.7 \times 10^{-19} \text{ cm}^2$ , for the  $\pi$  polarization, and  $1.4 \times 10^{-19} \text{ cm}^2$  up to  $2.6 \times 10^{-19} \text{ cm}^2$ , for the  $\sigma$  polarization [12,18–20].

## 5. Conclusion

We have presented a simple method to the in situ determination of the effective stimulated emission cross-section, based on the analysis of the output power as a function of the output reflectivity, in c.w. pumped lasers. The use of an acousto-optical modulator allows the controlled variation of the output reflectivity. Since the modulator is permanently located inside the resonator during the measurements, the spatial beam profile is preserved. Also, the total time taken for a complete measurement is shorter than any laser short term instability. This method was applied to the Nd:YLF laser, where the  $\sigma$  (1053 nm) and  $\pi$  (1047 nm) emission cross sections were determined. We have demonstrated that the emission cross-section can be obtained from an elementary laser oscillation model, being the obtained value in agreement with the results of a second determination, based on the analysis of the gain from the pumping conditions. The precision of both determinations was around 10%, what is better than the most part of previously reported determinations. Finally, there was not observed any dependence of the cross section on the power density levels studied.

## Acknowledgements

This work was supported by Fundação de Amparo à Pesquisa do Estado de São Paulo (FAPESP) under Grant 93/4999-7. The work of E.P. Maldonado is supported by a Ph.D. scholarship from FAPESP, under Grant 91/3968-5.

## References

- [1] J.K. Neeland and V. Evtuhov, *Phys. Rev.* 156 (1967) 244.
- [2] T. Kushida, H.M. Marcos and J.E. Geusic, *Phys. Rev.* 167 (1968) 289.
- [3] D.E. McCumber, *Phys. Rev.* 136 (1964) A954.
- [4] B.F. Aull and H.P. Janssen, *IEEE J. Quantum Electron.* 18 (1982) 925.
- [5] W. Koechner, *Solid-State Laser Engineering* (Springer, New York, 1986).
- [6] S.A. Payne, L.L. Chase, H.W. Newkirk, L.K. Smith and W.F. Krupke, *IEEE J. Quantum Electron.* 24 (1988) 2243.
- [7] S.A. Payne, J.A. Caird, L.L. Chase, L.K. Smith, N.D. Nielsen and W.F. Krupke, *J. Opt. Soc. Am. B* 8 (1991) 726.
- [8] W.E. Martin and D. Milam, *IEEE J. Quantum Electron.* 18 (1982) 1155.
- [9] K. Fuhrmann, N. Hodgson, F. Hollinger and H. Weber, *J. Appl. Phys.* 62 (1987) 4041.
- [10] T.Y. Fan and R.L. Byer, *IEEE J. Quantum Electron.* 24 (1988) 895.
- [11] W.P. Risk, *J. Opt. Soc. Am. B* 5 (1988) 1412.
- [12] N. Mermilliod, R. Romero, I. Chartier, C. Garapon and R. Moncorgé, *IEEE J. Quantum Electron.* 28 (1992) 1179.
- [13] E.P. Maldonado, G.E.C. Nogueira and N.D. Vieira Jr., *IEEE J. Quantum Electron.* 29 (1993) 1218.
- [14] Quantronix Acousto-Optic Q Switcher, model 303.
- [15] A.L. Harmer, A. Linz and D.R. Gabbe, *J. Phys. Chem. Solids* 30 (1969) 1483.
- [16] L.W. Casperson, *Appl. Optics* 19 (1980) 422.
- [17] N.D. Vieira Jr. and L.F. Mollenauer, *IEEE J. Quantum Electron.* 21 (1985) 195.
- [18] J.R. Ryan and R. Beach, *J. Opt. Soc. Am. B* 9 (1992) 1883.
- [19] H.Y. Shen, R.R. Zheng, Y.P. Zhou, G.F. Yu, C.H. Huang, Z.D. Zeng, W.J. Zhang and Q.J. Ye, *Appl. Phys. Lett.* 56 (1990) 1937.
- [20] A.A. Kaminskii, *Laser Crystals* (Springer, New York, 1981).